



available at [www.sciencedirect.com](http://www.sciencedirect.com)



journal homepage: [www.elsevier.com/locate/jhydrol](http://www.elsevier.com/locate/jhydrol)



# Monitoring daily evapotranspiration at a regional scale from Landsat-TM and ETM+ data: Application to the Basilicata region

J.M. Sánchez <sup>a,\*</sup>, G. Scavone <sup>b</sup>, V. Caselles <sup>a</sup>, E. Valor <sup>a</sup>, V.A. Copertino <sup>b</sup>, V. Telesca <sup>b</sup>

<sup>a</sup> Earth Physics and Thermodynamics Department, Faculty of Physics, University of Valencia, 50 Dr. Moliner, 46100 Burjassot, Spain

<sup>b</sup> Department of Engineering and Environmental Physics, University of Basilicata, Potenza, Italy

Received 1 June 2007; received in revised form 4 October 2007; accepted 19 November 2007

## KEYWORDS

Evapotranspiration;  
Sensible heat flux;  
Net radiation;  
STSEB;  
Landsat

**Summary** The increasing interest of hydrological, climatic and meteorological models in the different components of the surface energy balance has encouraged the development of operational methods for estimating surface energy fluxes at a regional scale. In this paper, a sequence of three high-resolution satellite-based surface energy fluxes images are analyzed over an extensive area with a large variety of land uses. Two images from Landsat 7-ETM+ (1999, 2002) and one from Landsat 5-TM (2004) are collected covering the whole Basilicata region (Southern Italy). A Simplified version of a Two-Source Energy Balance (STSEB) model is used to retrieve the surface sensible heat flux. A balance between the long-wave and short-wave radiation is applied to extract the net radiation flux. The evapotranspiration ( $LE$ ) is obtained as a residual term of the energy balance equation. The different croplands are characterized from the CORINE Land Cover maps, and the required meteorological variables are obtained by interpolating the data of a network of agro-meteorological stations distributed within the region. Atmospheric profiles from radiosoundings are used in the radiative transfer model MODTRAN 4.0 to correct the satellite data. Maps of the different fluxes are produced. Daily  $LE$  results are compared with some ground measurements, and an analysis is made taking the land use classification as a basis. An accuracy close to  $1 \text{ mm day}^{-1}$  is obtained. This value is in agreement with the typical uncertainties reported in the literature.

© 2007 Elsevier B.V. All rights reserved.

\* Corresponding author. Tel.: +34 963543249.

E-mail address: [juan.m.sanchez@uv.es](mailto:juan.m.sanchez@uv.es) (J.M. Sánchez).

## Introduction

The physical characterization of the hydrological processes plays a very important role in the framework of the activities for the management of the hydrological resources. Particularly, the soil–vegetation–atmosphere energy exchanges are the basis of an appropriate hydrological balance, and thus, of an appropriate planning of the hydrological resources.

The fusion of physical models for estimating the hydrological balance, and particularly the evapotranspiration ( $LE$ ), with technological advances for the characterization of hydrological, hydro-geological, and atmospheric issues, is of great utility. Although there are several surface-based methods that can accurately measure surface heat fluxes at point locations, it is not feasible to use a network of these systems to create spatially distributed flux maps because of the high variability of real landscapes. As stated by Scott et al. (2000), micrometeorological approaches can only realistically provide measurements representative of a particular type of vegetation cover when there is a reasonably extensive, uniform area of that vegetation immediately upwind of the instruments. The use of remote sensing techniques supplies the frequent lack of ground-measured variables and parameters required to apply the local models at a regional scale. Modelling evapotranspiration is very sensitive to the surface features and conditions. For this reason, a regional model must account for the surface variability. In this context, satellite remote sensing has become a basic tool since it allows us the regular monitoring of extensive areas. Different surface variables and parameters can be extracted from the combination of the multi-spectral information contained in a satellite image. The surface can be characterized with a detail depending on the spatial resolution of the sensor used.

Inoue and Moran (1997) proposed a simple method to estimate daily values of actual canopy transpiration. The method utilizes instantaneous differences of canopy and air temperature around mid-day as a major input. Results were found to be well correlated to those measured by steam-flow heat balance method in soybean canopies. Anderson et al. (1997) presented an operational two-source (soil + vegetation) model for evaluating the surface energy balance given measurements of the time rate of change in radiometric surface temperature during morning hours. Using this model, the need for ancillary measurements of near-surface air temperature is eliminated. The performance of this model was evaluated in comparison with data collected during the first International Satellite Land Surface Climatology Project field experiment, in Kansas, and the Monsoon'90 experiment, conducted in southern Arizona. Comparisons yielded uncertainties comparable to measurement errors typical of standard micrometeorological methods for flux estimation. Chehbouni et al. (2001) used dual angle observations of radiative surface temperature in conjunction with a two-layer model to derive sensible heat flux over the Semi Arid Land Surface Atmosphere program (SALSA) in Mexico. The average error was about 23%. Moran et al. (1994) introduced a water deficit index for evaluating evapotranspiration rates of both full cover and partially vegetated sites. This index can be computed using remotely sensed measurements of surface tempera-

ture and reflectance with limited on-site meteorological data. Comparison with simulations of a two-source energy balance model showed accurate estimates of field evapotranspiration rates. French et al. (2005) used data from ASTER collected over an experimental site in central Iowa, in the framework of the Soil moisture Atmosphere Coupling Experiment (SMACEX), to retrieve surface energy fluxes. Two different approaches, designed to account for the spatial variability, were considered: the Two-Source Energy Balance model (TSEB) and the Surface Energy Balance Algorithm for Land model (SEBAL). Comparison of the results with eddy-covariance measurements showed better agreement using the TSEB model with average deviations lower than  $20 \text{ W m}^{-2}$ . These results were also supported by Li et al. (2005). These authors compared local model output using two different versions of the TSEB (series and parallel) with tower-based flux observations. Root mean square differences ranged from  $20$ – $50 \text{ W m}^{-2}$ . In this case, land surface temperatures were derived from high-resolution Landsat Thematic Mapper (TM) and Enhanced Thematic Mapper (ETM+) scenes and aircraft imagery. Su et al. (2005) used also SMACEX data to evaluate the Surface Energy Balance System (SEBS) model using both high-quality local scale data and high-resolution remote sensing data from the Landsat ETM+.

Several authors such as Moran et al. (1997), Kustas et al. (2004) or McCabe and Wood (2006) have studied the effect of the satellite spatial resolution on the surface energy fluxes retrieval. Moran et al. (1997) compared remotely sensed variables and energy balance components calculated in two ways: first, calculated at the pixel resolution and averaged to the coarser resolution; and second, calculated directly at the coarse resolution by aggregating the fine-resolution data to the coarse scale. These authors concluded that knowledge of the surface heterogeneity is essential for minimizing error in aggregation of surface fluxes. Kustas et al. (2004) examined the effect of sensor resolution on model output using Landsat data collected during SMACEX. The pixel resolution of the remote sensing inputs were varied from 60 m to 120 m, 240m, and 960 m. Comparison of the results with tower and aircraft-based flux measurements indicated that when the input resolution is lower than the length scale defining agricultural field boundaries across the landscape, variation in fluxes between different crop fields is not feasible. These results were also supported by McCabe and Wood (2006). These authors used data from Landsat ETM+, ASTER, and MODIS to independently estimate evapotranspiration during SMACEX. They observed a high degree of consistency between the retrievals from Landsat ETM+ and ASTER, as well as the utility of MODIS for regional scale evapotranspiration estimation.

Despite the wide variety of remote sensing-based works and proposed models on evapotranspiration retrieval, there is not a generalized agreement about the most appropriate model depending on the application area. In this paper, we present a methodology focused on the daily evapotranspiration retrieval ( $LE_d$ ) from high-resolution satellite data. The bases of this method are the energy balance equation and a Simplified Two-Source Energy Balance (STSEB) model proposed by Sánchez et al. (2007a) for estimating instantaneous surface fluxes. This model was validated over a

variety of surface conditions with good results. An exhaustive analysis of sensitivity to typical uncertainties (assumed for a regional variability) in the required inputs was performed by these authors.

The proposed method was applied to the Basilicata region, in the South of Italy. This is a challenging region since it covers an extensive area with a large variety of land uses. The different surface features were characterized from the CORINE Land Cover land use maps (APAT, 2005), and the required meteorological variables were obtained by interpolating the data of about forty agro-meteorological stations distributed within the region. Atmospheric profiles from radiosoundings were used in the radiative transfer model MODTRAN 4.0 (Berk et al., 1999) to correct the satellite data. Three satellite images were selected for this work, two from the Landsat 7-ETM+ (September 26th 1999 and June 14th 2002), and one from the Landsat 5-TM (May 26th 2004).

The goal of this study is the inclusion of a new approach to estimate the sensible heat flux, part of the STSEB model, in the traditional relationship of Seguin and Itier (1983). The result of this combination is a new methodology to retrieve daily evapotranspiration at a regional scale from remote sensing and meteorological data. In this paper, we focus on the application of this methodology to Landsat imagery but it could be extended to other high-resolution sensors.

This paper is organized as follows. The section "Methodology" provides the framework of the method and a summary of the STSEB model, as well as details of the retrieval of the model inputs. The study region and data used in this study are described in the section "Study site and measurements". In the section "Results and discussion", the results of  $LE_d$  are discussed and compared with ground measurements. Finally, conclusions are given in the section "Conclusions".

## Methodology

The governing equation is the Energy Balance Equation (EBE) of the land surface, which models a system formed by vegetation, surrounding soil, and atmosphere:

$$R_n = G + H + LE \quad (1)$$

where  $R_n$  is the net radiation flux ( $W m^{-2}$ ),  $G$  is the soil heat flux ( $W m^{-2}$ ),  $H$  is the sensible heat flux ( $W m^{-2}$ ) and  $LE$  is the latent heat flux in the atmosphere boundary layer ( $W m^{-2}$ ). According to Seguin and Itier (1983)

$$\frac{H_d}{R_{nd}} = \frac{H_i}{R_{ni}} \quad (2)$$

where the subscripts  $i$  and  $d$  refer to instantaneous and daily fluxes, respectively.

On diurnal timescales,  $G$  can constitute an important contribution to the EBE (Choudhury et al., 1987; Santanello and Friedl, 2003). However, at a daily scale  $G$  can be neglected in Eq. (1) (Seguin and Itier, 1983; Lagouarde and McAneney, 1992; Sánchez et al., 2007b), and  $LE$  can be obtained from Eqs. (1) and (2) as

$$LE_d = \frac{R_{nd}}{R_{ni}} (R_{ni} - H_i) \quad (3)$$

Using Eq. (3),  $LE_d$  can be obtained from the instantaneous values of  $R_n$  and  $H$  at a particular time of day, and the relative net radiation contribution at that time when global radiative exchange is integrated,  $R_{nd}/R_{ni}$ .

The net radiation is estimated by establishing a balance between the long-wave and the short-wave radiation

$$R_n = (1 - \alpha)S + \varepsilon L_{sky} - \varepsilon \sigma T_{rad}^4 \quad (4)$$

where  $S$  is the solar global radiation ( $W m^{-2}$ ),  $T_{rad}$  is the radiometric land surface temperature,  $\alpha$  is the surface albedo,  $\varepsilon$  is the surface effective emissivity, and  $\sigma$  is the Stefan–Boltzmann constant.  $L_{sky}$  is the incident long-wave radiation ( $W m^{-2}$ ).

In the STSEB approach proposed in Sánchez et al. (2007a), the ground surface is divided in two components, canopy and soil surrounding. According to this configuration, the total sensible heat flux is obtained by the addition between the soil and canopy contributions,  $H_s$  and  $H_c$ , respectively:

$$H = P_v H_c + (1 - P_v) H_s \quad (5)$$

In this equation,  $H_s$  and  $H_c$  are expressed as

$$H_c = \rho C_p \frac{T_c - T_a}{r_a^h} \quad (6a)$$

$$H_s = \rho C_p \frac{T_s - T_a}{r_a^a + r_a^s} \quad (6b)$$

where  $\rho C_p$  is the volumetric heat capacity of air ( $J K^{-1} m^{-3}$ ),  $T_a$  is the air temperature at a reference height (K),  $T_c$  and  $T_s$  are the canopy and soil radiometric temperatures, respectively,  $r_a^h$  is the aerodynamic resistance to heat transfer between the canopy and the reference height ( $s m^{-1}$ ),  $r_a^a$  is the aerodynamic resistance to heat transfer between the point  $z_0+d$  ( $z_0$ : roughness length,  $d$ : displacement height) and the reference height ( $s m^{-1}$ ),  $r_a^s$  is the aerodynamic resistance to heat flow in the boundary layer immediately above the soil surface ( $s m^{-1}$ ). A summary of the expressions to estimate these resistances, and more details about the STSEB model can be seen in Sánchez et al. (2007a). A scheme of the methodology proposed in this paper is shown in Fig. 1.

## Surface temperature and emissivity

Landsat-TM and ETM+ sensors possess a unique thermal band with a spectral range of 10.4–12.5  $\mu m$ , and an effective wavelength of 11.457  $\mu m$ . This limitation does not allow to apply split-window methods neither Temperature/Emissivity Separation (TES) methods. Therefore, a single-channel method, based on the radiative transfer equation, was used. The remotely measured channel radiance,  $R_i$ , consist of two main contributions: (1) the radiance at surface level, which is attenuated by the absorption of the atmosphere between the surface and the instrument, characterized by the atmospheric transmittance,  $\tau_i$ , and (2) the upwelling sky radiance emitted by the atmosphere in the viewing direction,  $L_{i\text{atm}}^\uparrow(\theta)$ , so that  $R_i$ , in agreement with the radiative transfer equation, is stated as

$$R_i = [\varepsilon_i B_i(T_{rad}) + [1 - \varepsilon_i] L_{i\text{atm hem}}^\downarrow] \tau_i + L_{i\text{atm}}^\uparrow \quad (7)$$

where  $B_i(T_{rad})$  is Planck's function for a temperature  $T_{rad}$ ,  $\varepsilon_i$  is the surface emissivity and  $L_{i\text{atm hem}}^\downarrow$  is the hemispheric downwelling sky irradiance divided by  $\pi$  (Lambertian

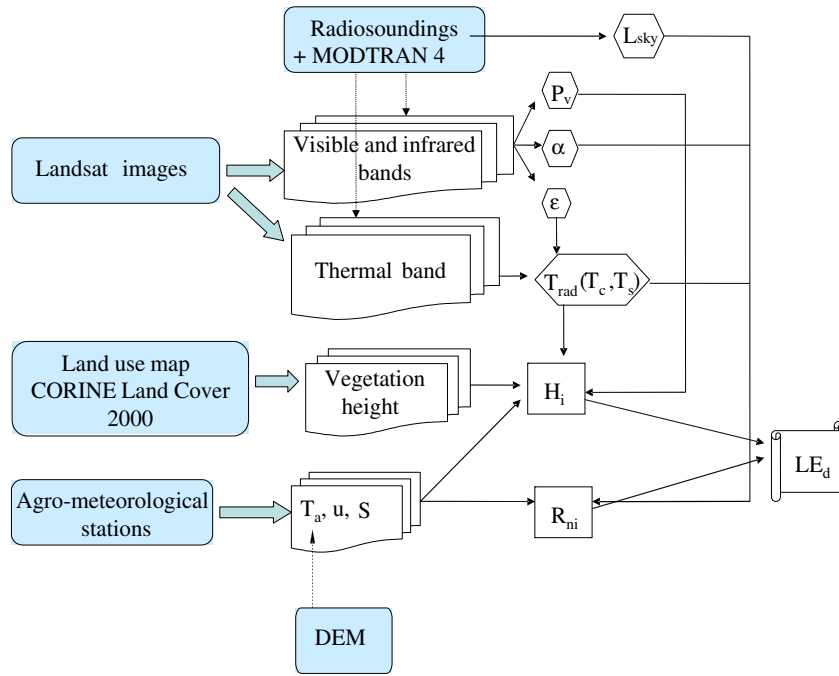


Figure 1 Scheme of the methodology proposed to retrieve actual daily evapotranspiration at a regional scale.

reflection assumed). Radiosounding data were introduced into the MODTRAN 4.0 code (Berk et al., 1999) to get estimates of  $\tau_i$ ,  $L_{i\text{atm}}^\uparrow(\theta)$  and  $L_{i\text{atm hem}}^\downarrow$ . Although Eq. (7) depends on the observation angle ( $\theta$ ), the nadir view provides good results for Landsat-TM and ETM+. A simple and operational equation proposed by Valor and Caselles (2005) was used to estimate the surface emissivity from the knowledge of the vegetation cover,  $P_v$ , and the emissivities of the soil and canopy components,  $\epsilon_s$  and  $\epsilon_c$ , respectively.

$$\epsilon = \epsilon_c P_v + \epsilon_s (1 - P_v) (1 - 1.74 P_v) + 1.7372 P_v (1 - P_v) \quad (8)$$

Eq. (8) includes the effect of the geometrical distribution of the vegetated surface and also the internal reflections. Typical emissivity values can be assumed for  $\epsilon_c$  and  $\epsilon_s$ .

### Vegetation cover

Bands 3 (0.63–0.69  $\mu\text{m}$ ) and 4 (0.76–0.90  $\mu\text{m}$ ) of TM and ETM+ were used to estimate NDVI. Previously, visible and near-infrared bands were corrected of atmospheric effects using the radiosounding data and the MODTRAN 4.0 code. For this purpose, the at-surface channel reflectivity,  $\rho_i$ , is calculated with the following equation:

$$\rho_i = \frac{\pi(R_i - L_{i\text{atm}}^\uparrow)d^2}{\tau_i(ESUN_i \cos(\alpha)\tau(\alpha) + L_{i\text{atm hem}}^\downarrow)} \quad (9)$$

where  $\tau(\alpha)$  is the atmospheric transmissivity between the sun and the surface,  $\alpha$  is the zenithal solar angle,  $ESUN_i$  is the spectral solar irradiance on the top of the atmosphere, and  $d$  is the Earth–Sun distance.

Vegetation cover was obtained through the expression (Valor and Caselles, 1996):

$$P_v = \frac{\left(1 - \frac{\text{NDVI}}{\text{NDVI}_s}\right)}{\left(1 - \frac{\text{NDVI}}{\text{NDVI}_s}\right) - K\left(1 - \frac{\text{NDVI}}{\text{NDVI}_s}\right)} \quad (10)$$

where the coefficient  $K$  is obtained by

$$K = \frac{R_{\text{NIR}_v} - R_{\text{RED}_v}}{R_{\text{NIR}_s} - R_{\text{RED}_s}} \quad (11)$$

where  $R_{\text{NIR}}$  is the near-infrared reflectivity, and  $R_{\text{RED}}$  is the red visible reflectivity. The subscript  $v$  and  $s$  correspond to completely vegetated and unvegetated areas, respectively, selected by looking at the spectral contrast among bands 3–5. These selected areas were also used to estimate  $T_c$  and  $T_s$ , required in Eqs. (6a) and (6b), respectively, from the land surface temperature maps generated.

### Albedo

Some authors such as Dubayah (1992), Duguay (1992), etc. divided the spectral region from 0.3 to 3.0  $\mu\text{m}$  into 10 spectral bands to estimate surface albedo. Each band has a different integrating weight according to the typical vegetation spectral reflectance pattern. In this paper, the surface albedo is integrated by using the equation (Dubayah, 1992):

$$\alpha = 0.221\rho_1 + 0.162\rho_2 + 0.102\rho_3 + 0.354\rho_4 + 0.059\rho_5 + 0.0195\rho_7 \quad (12)$$

where  $\rho_i$  is the corrected reflectivity for the  $i$  band of TM or ETM+. The average error of the calculated surface net radiation, using Eq. (12) for estimating the albedo, is around 2% when comparing to field measurements (Dubayah, 1992).

### Meteorological variables

Ancillary meteorological data are required to complete the set of variables and parameters involved in the previously shown scheme of equations. Air temperature,  $T_a$ , is necessary in Eqs. (6a) and (6b) to estimate the exchange of sen-

sible heat flux between the surface and the atmospheric boundary layer. Wind speed,  $u$  ( $\text{m s}^{-1}$ ), is required in the expressions to calculate the aerodynamic and soil resistances taking part in the STSEB model (Sánchez et al., 2007a). The global solar radiation,  $S$ , and the incident long-wave radiation,  $L_{\text{sky}}$ , are necessary in the net radiation balance (Eq. (4)). Since all these variables, except  $L_{\text{sky}}$ , are

continuously registered in typical agro-meteorological stations, regional maps can be created by interpolating the data registered in a network of stations distributed within the study area. Regarding  $L_{\text{sky}}$ , due to its known spatial homogeneity across a relative extensive area (Humes et al., 2002), a single value of this variable can be used for each image, and it can be obtained from launched radiosoundings.

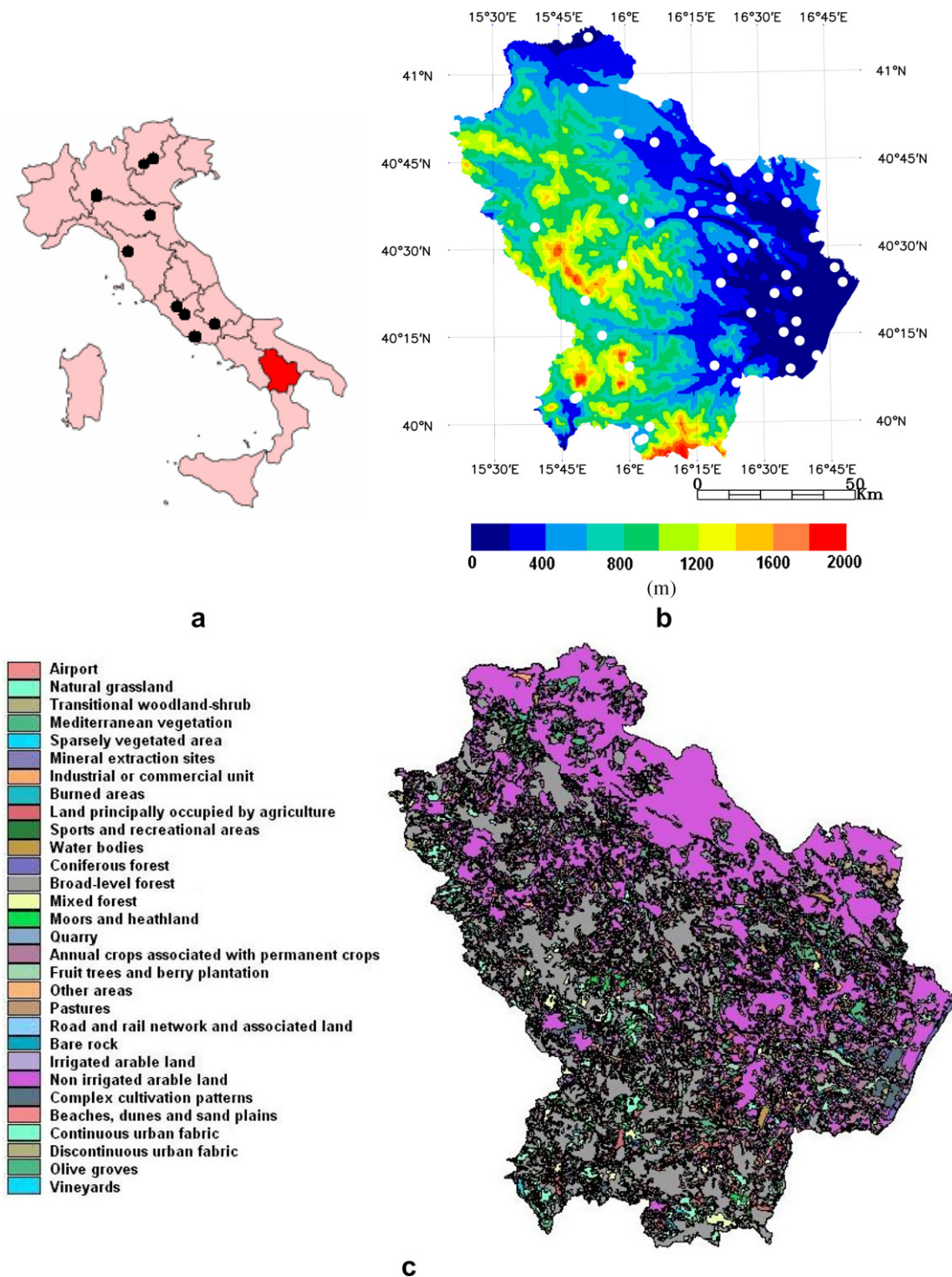


**Figure 2** (a) Location of the Basilicata region (in red colour) and the CarboEurope flux towers (black dots) within Italy, (b) Digital elevation model of the Basilicata region. The white dots indicate the exact location of the agro-meteorological stations used and (c) Land use map of the Basilicata region (CORINE Land Cover 2000 project).

In this paper, a geostatistical technique (kriging) was used to interpolate the data of a regional network of agro-meteorological stations, and elaborate wind speed and global solar radiation maps. Sánchez et al. (2007a) showed that particular care must be taken with the air temperature when the STSEB model is applied since an uncertainty in  $T_a$  can lead to a significant error in the evapotranspiration retrieval. For this reason a Digital Elevation Model (DEM) was considered and the relationship between the air temperature and the altitude above sea level was established in order to obtain more reliable maps of this meteorological variable.

## Study site and measurements

### The Basilicata region

Placed in the South of Italy, Basilicata is a 9992 km<sup>2</sup> region (Fig. 2a), divided in two provinces: Potenza and Matera. It is a prevalently mountainous region. In fact, mountains take up the 47% of the territory (areas above 700 m a.s.l.), hills take up the 45% (areas between 201 and 700 m a.s.l.) and plains just the 8% (areas below 200 m a.s.l.). The western mountainous part of the region can be distinguished from the coastal and the hilly central ones, which extends as far as the arid *Murgia* of Matera. Fig. 2b shows the DEM, obtained from MODIS, used in this work.

The wide variety of land uses in this region makes it appropriate for an analysis of the method performance in evapotranspiration retrieval under different surface conditions. A land use map from the CORINE Land Cover project (Fig. 2c) was used to characterize the surface with nominal values of canopy height for each land use. Analysing the peculiarities of the vegetation, strongly influenced by climatic conditions of the zone, the region can be considered divided in two parts. The Western part, along the strip of the Apennine, is characterized by highly vegetated soils, with many woods and fields under cultivation of vines and olive. The Eastern part of the region, instead, is characterized by bare and arid soils, with poor vegetation, except some irrigated zones with cultivations of oranges, peaches, strawberries, etc.

### Ground measurements

A network of 38 agro-meteorological stations distributed within the region (Fig. 2b) and managed by ALSIA (Agenzia Lucana di Sviluppo ed Innovazione in Agricoltura – Agriculture Development and Innovation Agency of Lucania) are equipped with instruments for automatic and continuous measurements of various meteorological parameters, such as air temperature, relative humidity, global solar radiation, soil temperature, speed and direction of wind, precipitation and potential evapotranspiration. Air temperature is measured by PT100 thermo-resistances with a precision of  $\pm 0.1$  °C. Solar radiation is measured through pyranometers working in the range 0.3–2.5  $\mu\text{m}$  with an accuracy of  $\pm 2\%$ . The instruments used for the survey of the horizontal component of the wind speed are classic cup-anemometers, with an accuracy of  $\pm 0.5$  m s<sup>-1</sup>.

Finally, two weighing lysimeters placed at two different cropland sites, Lavello (41°6'6"N, 15°50'55"E) and Policoro

(40°10'15"N, 16°38'53"E), registered actual  $LE_d$  values. These weighing lysimeters consist of a filled in cultivation tank, with an area of 2 m  $\times$  2 m and a depth of 1.30 m, isolated from any external structure. Water consumptions and daily evapotranspiration are obtained directly by the difference in weight between two subsequent readings. The resolution of this system is about 0.06 mm. Experimental Demonstrative Farm of Gaudio – Lavello (PZ) provided us with *in situ* lysimeter data, collected by the University of Basilicata, corresponding to: September 26th 1999 and June 14th 2002, on an aubergine and tomato growing, respectively. Evapotranspiration data corresponding to September 26th 1999, on a radish growing, and June 14th 2002, on a tomato growing, were provided by the Food Production Science Institute of Bari, which is responsible for collecting data coming from Experimental Farm "E. Pantanelli" of Policoro (MT).

### The Landsat images

Three cloud-free Landsat images were selected for this work, one corresponding to the TM sensor, on-board Landsat 5, (hereafter referred to as L5-TM) (May 26th 2004), and two corresponding to the ETM+ sensor, on-board Landsat 7 (hereafter referred to as L7-ETM+) (September 26th 1999 and June 14th 2002). The high spatial resolution of these sensors (30-m in visible and near-infrared bands, and 60-m for L7-ETM+ or 120-m for L5-TM in the thermal band) allows a detailed monitoring of the surface features, required in the methodology described, for the whole Basilicata region.

## Results and discussion

In this section, we present the application of the methodology given in the section "Methodology" for retrieving  $LE_d$  from Landsat imagery. At the end of the section, results will be compared with some *in situ* measurements.

Atmospheric profiles, from radiosoundings launched in a nearby area were processed for each date using the MODTRAN 4.0 code. As explained in the Section "Vegetation cover", visible and near-infrared bands were corrected, and a NDVI map was elaborated from each Landsat image. A careful searching process was carried out, based on the contrast shown in bands 3 and 4, and on the obtained NDVI, so as to identify completely vegetated and completely bare pixels. Several samples of each class were selected distributed around the whole region in order to account for the spatial variability within the area. Average values of these samples were used for the soil and canopy parameters in Eqs. (10) and (11) (see Table 1). Fig. 3a–c shows the vegetation cover maps obtained from the three images. Note that the image corresponding to June 2002 shows the highest  $P_v$  values overall. Also, the highest  $P_v$  values are easily identified with forested areas looking at Fig. 2c. As explained in the section "Surface temperature and emissivity", emissivity maps were obtained by applying Eq. (8) assuming nominal values of  $\varepsilon_c = 0.985$  and  $\varepsilon_s = 0.960$ . Table 1 summarizes the atmospheric parameters obtained from radiosounding data for each date, required in the radiative transfer equation. Fig. 3d–f shows the produced maps of land surface temperature. Some authors such as Sobrino

**Table 1** Atmospheric parameters estimated from radiosounding data and the MODTRAN 4.0 code, and soil and canopy parameters used in Eqs. (10) and (11)

Image	$\tau_i$	$L_{i\text{atm}}^{\uparrow}$ ( $\text{W m}^{-2}\text{Sr } \mu\text{m}$ )	$L_{i\text{atm hem}}^{\downarrow}$ ( $\text{W m}^{-2}\text{Sr } \mu\text{m}$ )	$L_{\text{sky}}$ ( $\text{W m}^{-2}$ )	$R_{\text{NIR}_v}$	$R_{\text{NIR}_s}$	$R_{\text{RED}_v}$	$R_{\text{RED}_s}$	NDVI <sub>v</sub>	NDVI <sub>s</sub>
L7-ETM+ (09/26/1999)	0.735	2.088	3.142	337	0.521	0.319	0.059	0.309	0.794	0.020
L7-ETM+ (06/14/2002)	0.811	1.433	2.198	332	0.689	0.397	0.010	0.227	0.980	0.274
L5-TM (05/26/2004)	0.813	1.325	2.019	312	0.570	0.190	0.043	0.103	0.861	0.307

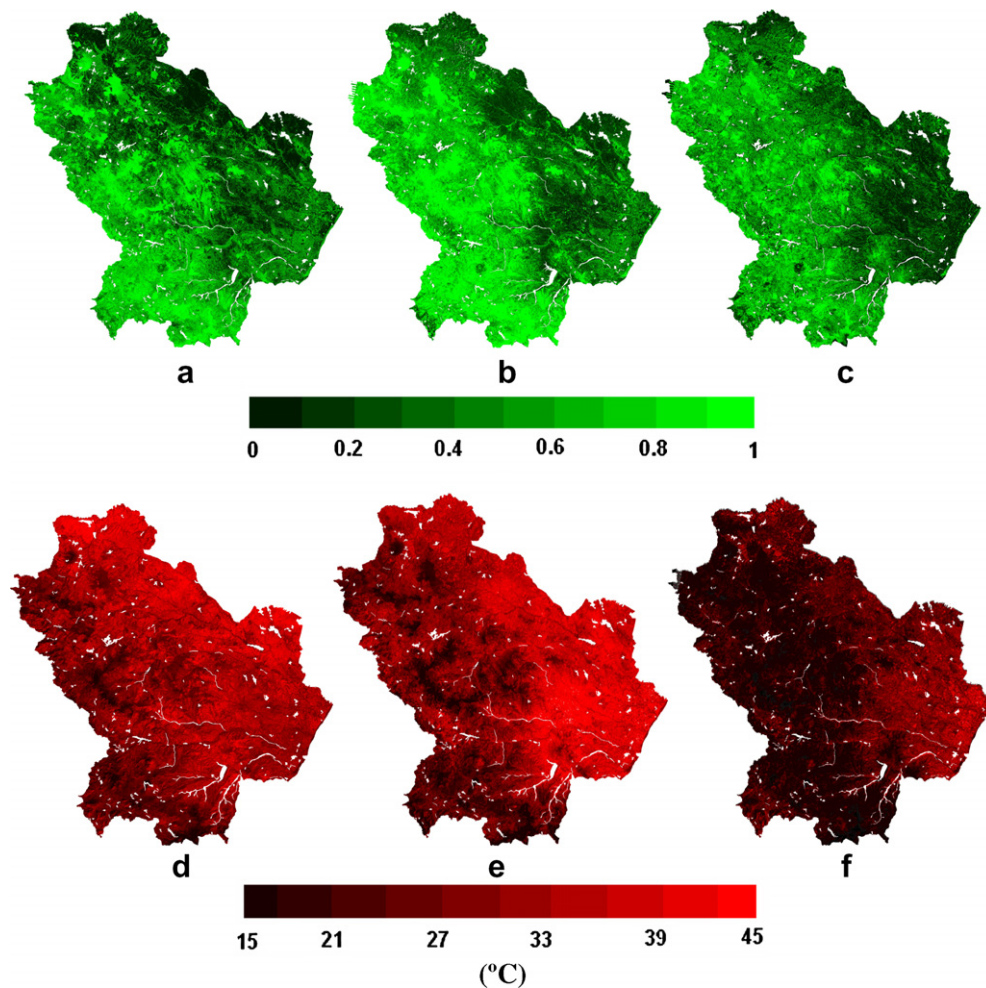


**Figure 3** Vegetation cover,  $P_v$ , maps obtained by applying Eqs. (10) and (11) to the NDVI map; (a) 09/26/1999, (b) 06/14/2002, (c) 05/26/2004, and Land surface temperature,  $T_{\text{rad}}$  ( $^{\circ}\text{C}$ ), maps obtained by applying Eq. (7); (d) 09/26/1999, (e) 06/14/2002, and (f) 05/26/2004.

et al. (2004) and Li et al. (2005) have shown the validity of the Land Surface Temperature (LST) obtained from Landsat 5-TM and Landsat 7-ETM+, respectively, using the radiative transfer equation, with errors lower than  $1^{\circ}\text{C}$ . This uncertainty is acceptable for the accuracy in  $LE$  of the STSEB model as shown in Sánchez et al. (2007a), where the sensitivity of the model was studied assuming uncertainties of  $1^{\circ}\text{C}$  and  $2^{\circ}\text{C}$  for the canopy and soil temperatures, respectively.

A list of the agro-meteorological stations used in this work is shown in Table 2 (see also Fig. 2b). The air temperature maps were obtained by extrapolating the relationship

deduced between the stations  $T_a$  and altitude above sea level data to the whole region from the DEM information. Root Mean Square Difference (RMSD) values close to  $1^{\circ}\text{C}$  were obtained in all cases. This is also the uncertainty assumed by Sánchez et al. (2007a) for studying the sensitivity of the STSEB model to the  $T_a$  input. A kriging interpolation was used to elaborate wind speed and global solar radiation maps as stated in the section ‘‘Meteorological variables’’.

The integrated surface albedo was estimated using Eq. (12). Previous emissivity results using Eq. (8) were also used in Eq. (4) since some authors such as Ogawa et al. (2002) showed that emissivity in the range  $8\text{--}14\ \mu\text{m}$  is well-repre-

**Table 2** List of the agro-meteorological stations distributed around the Basilicata region

No.	Station	Altitude a.s.l. (m)	Lat N	Lon E
1	GE1	320	40°47'57"	16°05'39"
2	MO6	92	40°15'07"	16°34'00"
3	LAU	938	40°27'03"	15°58'07"
4	BG1	595	40°20'58"	15°49'43"
5	ACE	420	40°49'32"	15°57'36"
6	ME3	68	40°26'02"	16°45'40"
7	GR1	190	40°35'49"	16°14'11"
8	GRU	520	40°36'20"	16°22'37"
9	GRD	191	40°38'24"	16°22'38"
10	MO4	154	40°16'52"	16°36'53"
11	SMF	450	40°27'59"	16°22'47"
12	FER	314	40°30'25"	16°27'34"
13	CRP	51	40°21'48"	16°32'08"
14	SGL	455	40°06'37"	16°23'16"
15	CMP	824	40°34'08"	16°04'17"
16	NS3	152	40°08'52"	16°35'21"
17	PI1	192	40°21'52"	16°37'13"
18	PI3	52	40°24'52"	16°34'47"
19	PO1	117	40°13'33"	16°37'32"
20	MTP	262	40°41'41"	16°31'06"
21	PO3	6	40°11'00"	16°41'17"
22	NEM	500	40°04'30"	15°47'48"
23	BRM	820	40°38'20"	15°58'25"
24	STI	240	40°23'42"	16°20'03"
25	MTS	45	40°31'23"	16°41'50"
26	VIG	616	39°59'15"	16°03'45"
27	CSR	1010	40°09'37"	15°59'25"
28	ROT	640	39°57'14"	16°02'14"
29	SAR	662	40°14'56"	15°53'22"
30	SMI	450	40°44'52"	16°19'53"
31	LAV	180	41°06'06'	15°50'55"
32	ALI	190	40°18'28"	16°26'48"
33	MTQ	200	40°37'22"	16°35'05"
34	SAT	700	40°33'34"	15°38'34"
35	SEN	270	40°09'36"	16°18'27"
36	ROS	635	39°57'14"	16°02'24"
37	PAN	24	40°23'28"	16°47'25"
38	VEN	415	40°57'21"	15°49'38"

Their location on the map can be observed in Fig. 2b.

sentative of the total emissivity value. Table 1 includes the values of  $L_{sky}$  used in the long-wave radiation balance. Finally, Fig. 4a–c shows the net radiation maps. Comparing Figs. 4 and 3, it can be seen that the highest  $R_{ni}$  values are obtained for the most vegetated areas, and the lowest for the bare areas. After estimating the values of  $T_c$  and  $T_s$  according to the aforesaid procedure, maps of sensible heat flux were produced (Fig. 4d–f). At the Landsat overpass times,  $T_{rad}$  is typically higher than  $T_a$  for most landscapes (positive  $H$ ) (Moran et al., 1997). It is possible that under some particular surface conditions  $T_a$  is slightly higher than  $T_{rad}$ , yielding slightly negative values of  $H$ . However, the produced maps of air temperature and wind speed, inputs in the retrieval of the sensible heat flux, may contain spatial uncertainties that might lead to excessive and unrealistic negative values of  $H$ . For this reason, regions showing

$H < -50 \text{ W m}^{-2}$  have been masked out and not considered in the current analysis.  $R_{nd}/R_{ni}$  values in Eq. (3) were calculated for each date from the ground-collected data. Since the ratio  $R_{nd}/R_{ni}$  has been shown to vary with the time, date, or the site latitude, but not with the vegetation type (Sobrino et al., 2005; Sánchez et al., 2007b), a constant value was used for each image: 0.365, 0.378, and 0.351 for the images L7\_99, L7\_02, and L5\_04, respectively. Finally, Fig. 4g–i shows the produced  $LE_d$  maps ( $\text{mm day}^{-1}$ ). As a consequence of the aforementioned uncertainties in the meteorological variables, some unrealistic negative values of daily evapotranspiration were obtained, provoked by excessive and unrealistic high values of  $H$ . Those correspond to areas above approximately 1500 m altitude, according to the DEM. This portion of pixels has been also masked out in Fig. 4d–i. Overall, it can be seen that the highest  $LE_d$  values were obtained for the most vegetated areas, while the lowest for the bare areas. However, there is also a small portion of pixels with high  $P_v$  values and low  $LE_d$  values. Those correspond to high elevation areas with cooler  $T_a$ , resulting in high values of  $H$ . For a quantitative analysis of the regional  $LE_d$  results, average values of all pixels within each land use have been calculated. Table 3 shows a list of these results for the main land uses. Coniferous and broad-leaf forests, together with fruit trees and agriculture areas, show generally the highest values. Meanwhile, sparsely vegetated areas, arable lands, or pastures show the lowest  $LE_d$  values. Overall, daily evapotranspiration values in May 2004 are the highest, and those in September 1999 are the lowest. The mean  $LE_d$  values for the whole region result 4.5, 4.0, and  $3.1 \text{ mm day}^{-1}$  for May 2004, June 2002, and September 1999, respectively.

Histograms of  $LE_d$  results were elaborated for three of the most dominant land uses within the Basilicata region (Fig. 5a–c). Fig. 5a shows the histogram corresponding to arable lands. Mean values with their standard deviations result in  $2.4 \pm 1.0 \text{ mm day}^{-1}$ ,  $3.6 \pm 1.4 \text{ mm day}^{-1}$ , and  $4.6 \pm 1.0 \text{ mm day}^{-1}$ , for September 1999, June 2002, and May 2004, respectively. Note that the maximum values of the distributions are clearly separated, and that the standard deviation for June 2002 is greater than for the other dates. Fig. 5b shows the histogram corresponding to broad-leaf forest. Now, the mean values are  $4.2 \pm 1.3 \text{ mm day}^{-1}$ ,  $4.8 \pm 1.8 \text{ mm day}^{-1}$ , and  $4.5 \pm 1.6 \text{ mm day}^{-1}$ , for September 1999, June 2002, and May 2004, respectively. This time mean values are close and the standard deviation for June 2002 is again the greatest one. Finally, the histogram corresponding to natural grasslands is shown in Fig. 5c. The mean values result in  $3.4 \pm 1.0 \text{ mm day}^{-1}$ ,  $4.2 \pm 1.3 \text{ mm day}^{-1}$ , and  $4.8 \pm 1.0 \text{ mm day}^{-1}$ , for September 1999, June 2002, and May 2004, respectively. Once again, the greatest standard deviation is obtained for June 2002. This is the expected behaviour attending to the phenological stage of the vegetation if we make the assumption that environmental conditions for the three years are comparable. Typically, crops planted in the arable lands tend to suffer significant changes in their phenological stage from May (end of the spring) to September (beginning of the autumn). However, forested areas remain almost unchanged. Natural grasslands are in an intermediate situation. This explains the differences observed between the mean values of  $LE_d$  for different dates, but the greater value of standard devi-

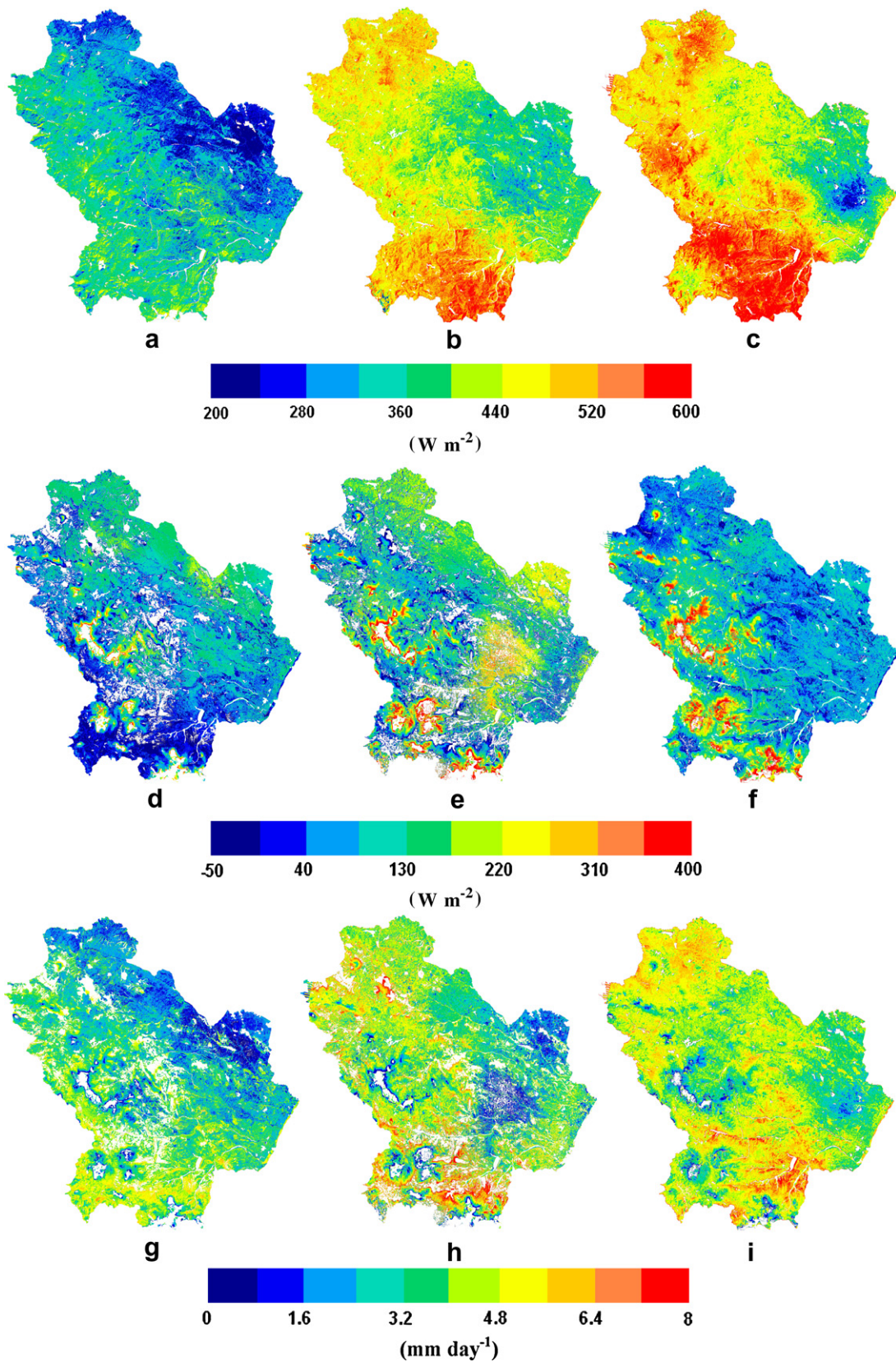


**Figure 4** Instantaneous net radiation flux,  $R_{ni}$  ( $\text{W m}^{-2}$ ), maps obtained through Eq. (4); (a) 09/26/1999, (b) 06/14/2002, (c) 05/26/2004, Instantaneous sensible heat flux,  $H_i$  ( $\text{W m}^{-2}$ ), maps obtained through Eqs. (5), (6a) and (6b); (d) 09/26/1999, (e) 06/14/2002, (f) 05/26/2004, and Actual daily evapotranspiration,  $LE_d$  ( $\text{mm day}^{-1}$ ), maps obtained by applying Eq. (3); (g) 09/26/1999, (h) 06/14/2002, and (i) 05/26/2004.

**Table 3** Average values of  $LE_d$  ( $\text{mm day}^{-1}$ ) for the main land uses

Land use	L7-ETM+ (09/26/1999)	L7-ETM+ (06/14/2002)	L5-TM (05/26/2004)
Pastures	2.9	3.3	4.1
Natural grassland	3.4	4.2	4.8
Fruit trees	3.8	4.5	4.3
Olives	3.3	4.0	4.1
Vineyards	3.4	4.4	4.4
Moors and heathland	3.3	3.9	4.1
Sparsely vegetated areas	2.8	2.7	3.7
Arable lands	2.4	3.6	4.6
Land princ. ocup. by agriculture	3.6	4.4	4.8
Annual crops	3.3	4.1	4.5
Complex cultivation patterns	3.4	4.0	4.3
Coniferous forests	4.3	4.8	5.2
Broad-leaf forests	4.2	4.8	4.5
Mixed forests	3.7	4.1	3.8
Whole region	3.1	4.0	4.5

ation for June 2002 is still unexplained. With this aim, an additional plot showing the histogram of the wind speed values for the whole area was produced (Fig. 5d). The mean values result in  $2.0 \pm 0.6 \text{ m s}^{-1}$ ,  $2.3 \pm 1.1 \text{ m s}^{-1}$ , and  $1.6 \pm 0.3 \text{ m s}^{-1}$  for September 1999, June 2002, and May 2004, respectively. An important variability of the wind speed around the whole region is observed for June 2002, against a relative homogeneity for September 1999 and May 2004. These results explain the wider distribution, and consequently, higher standard deviation value of the  $LE_d$  histograms corresponding to June 2002 for the three vegetation types analyzed. Similar discussions could be established for other land uses included in Table 4.

Note the low variability in  $LE_d$  results of the different land uses for the L5-TM image compared with the other two L7-ETM+ cases. The 120-m spatial resolution in the

**Table 4** Comparison between lysimeter measurements of  $LE_d$  ( $\text{mm day}^{-1}$ ) and results extracted from Fig. 4g–i, for the particular locations of the instruments

Date	Lysimeter	Measured	Estimated	Difference
September 26th 1999	Lavello	—	3.01	—
	Policoro	1.93	2.13	0.20
June 14th 2002	Lavello	2.17	3.22	1.05
	Policoro	2.87	3.01	0.14

Lavello datum for September 26th 1999 was not reliable, and no lysimeter data were available for May 26th 2004.

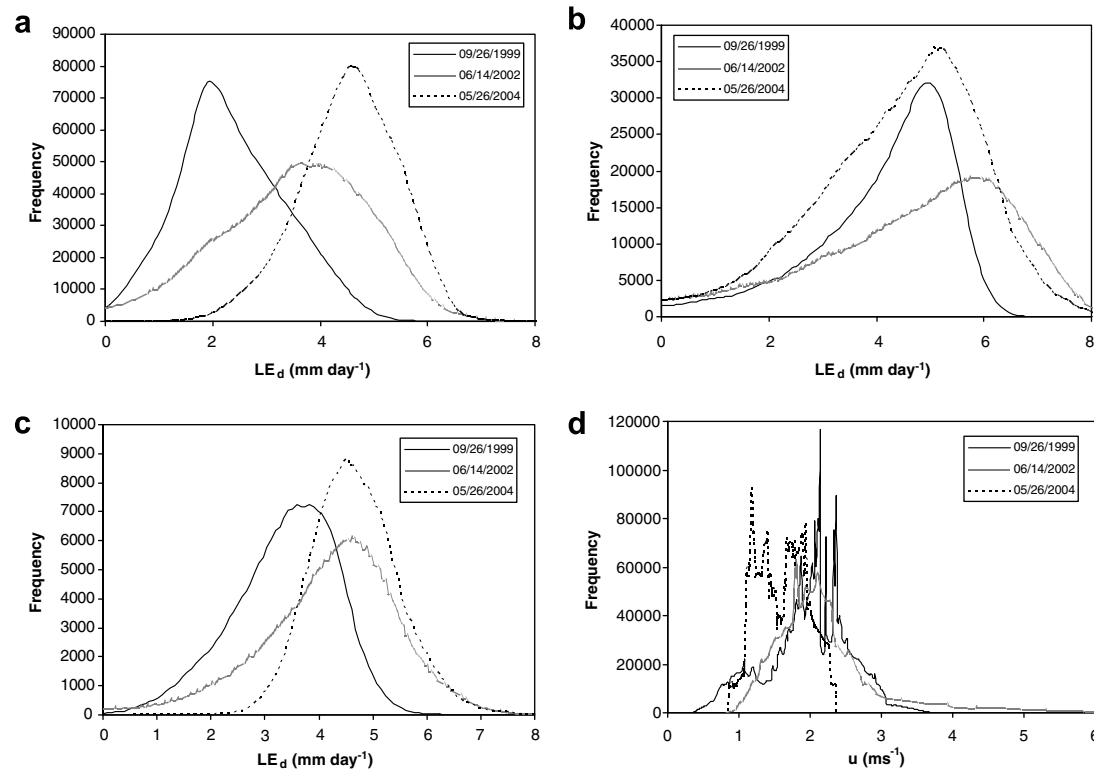


**Figure 5** Histograms to illustrate the variability of  $LE_d$  ( $\text{mm day}^{-1}$ ) for the three dates and the following land uses: (a) Arable land, (b) Broad-Level forest, (c) Natural grassland. (d) Histogram to illustrate the variability of  $u$  ( $\text{m s}^{-1}$ ) for the three dates and the whole Basilicata region.

thermal band of TM, compared with the 60-m of ETM+, can be significant for this fact.

To assess the performance of the described methodology,  $LE_d$  results were compared with some punctual lysimeter measurements. Table 4 shows the comparison between these measurements and the results obtained in Fig. 4 for the particular location of the two lysimeters. A RMSD value of  $\pm 0.7 \text{ mm day}^{-1}$  was obtained, with a maximum difference of  $1.05 \text{ mm day}^{-1}$ . To reinforce this assessment at a wider scale, data from the CarboEurope project dataset have been used. This is an international project which main objective is the study of the carbon dioxide exchanges between the surface and the atmosphere. For this aim, a network of towers, equipped with the instruments required for the direct measurement of the surface fluxes, has been distributed around Europe (see Table 5 and Fig. 2a). Ground-measured  $LE_d$  values from these towers were used to test the average values obtained using the land use classification over the Basilicata region. A RMSD value of  $\pm 1.0 \text{ mm day}^{-1}$  is obtained with an overestimation of  $0.5 \text{ mm day}^{-1}$ . Even though a more complete network of  $LE_d$  ground-measured values, spatially distributed around the study region and representative of the different land uses, would be desirable for a robust validation, the results obtained give some confidence on the proposed methodology to evaluate daily evapotranspiration at a regional scale.

Nagler et al. (2005) proposed a multivariate regression equation for predicting  $LE_d$  from  $EVI$  (Enhanced Vegetation Index) and  $T_a$ . Comparison with  $LE_d$  values measured by eddy-covariance method (Cleverly et al., 2002), over cottonwood and saltcedar along the Middle Rio Grande river corridor in New Mexico, showed estimation errors of about  $1.1 \text{ mm day}^{-1}$ . Gómez et al. (2005) assessed the potential

of the S-SEBI (Simplified Surface Energy Balance Index) method for estimating daily evapotranspiration. The method was implemented using data collected with two airborne sensors over the Alpillles ReSeDA (Remote Sensing Data Assimilation) experimental area. The validation showed an estimation error of  $1 \text{ mm day}^{-1}$ . A similar accuracy of  $1 \text{ mm day}^{-1}$  was obtained by Sobrino et al. (2005) when applying the S-SEBI model over the Barrax test site in Spain, in the framework of DAISEX (Digital Airborne Imaging Spectrometer Experiment) campaign. Ground values of  $LE_d$  were measured with two lysimeters placed on festuca and barley. Recently, Nagler et al. (2007) showed that cottonwood  $LE_d$  can be monitored by remote sensing methods calibrated with ground measurements with an accuracy or uncertainty of 20–30% in riparian corridors of western US rivers. Validation was established by comparison with sap flow measurements.

Note that the main aim of the present work is to show a feasible and, at the same time simple methodology, that allows us to retrieve  $LE_d$  at a regional scale assembling remote sensing and ground-measured data. More complicated techniques, involving a greater number of variables and parameters, and/or more tedious computation processes could have been introduced. However, the operability of the method would have been significantly reduced. Further work will deal with the study of the effect of possible improvements to the described methodology on the final  $LE_d$  results. For example:

- More sophisticated methods that incorporate geographical information, such as co-kriging and elevation-detrended kriging techniques can be applied to elaborate maps of the meteorological variables required. Also, a

**Table 5** Comparison between ground-measured values of  $LE_d$  ( $\text{mm day}^{-1}$ ) (eddy-correlation or Bowen ratio systems) in the CarboEurope Italian sites and results obtained for similar land uses over the Basilicata region

Site/date	Land cover	Lat./Long.	$LE_d$ measured	$LE_d$ estimated	Difference
Collelongo 09/26/1999	Mixed forest	41°50'58"N 13°35'17"E	2.0	3.7	1.7
San Rossore 06/14/2002	Coniferous forest	43°43'47"N 10°17'13"E	4.7	4.8	0.1
Roccaresp. 1 06/14/2002	Broad-leaf forest	42°24'29"N 11°55'48"E	4.4	4.8	0.4
Roccaresp. 2 06/14/2002	Broad-leaf forest	42°23'25"N 11°55'15"E	4.2	4.8	0.6
Castelpolzano 06/14/2002	Natural grassland	41°42'19"N 12°22'34"E	2.8	4.2	1.4
Nonantola 06/14/2002	Cropland	44°41'23"N 11°5'19"E	5.4	4.4	-1.0
Lavarone 05/26/2004	Coniferous forest	45°57'19"N 11°16'52"E	3.4	5.2	1.8
Parco Ticino 05/26/2004	Broad-level forest	45°12'3"N 9°3'40"E	5.0	4.5	-0.5
Monte Bond. 05/26/2004	Mixed forest	46°1'47"N 11°4'59"E	3.9	3.8	-0.1
				Bias	0.5
				$\sigma$	$\pm 1.0$
				RMSD	$\pm 1.0$

Locations of the flux towers, as well as information about the vegetation type over which they are located, are also included.

digital elevation model with a higher spatial resolution can be introduced to reduce errors in the interpolation of the air temperature.

- Recent works have dealt with the effects of subpixel heterogeneity on the fluxes estimation, and a disaggregation procedure has been proposed for estimating subpixel variations in radiometric surface temperature (Kustas et al., 2003). This technique can be applied to Landsat images and derive  $T_{\text{rad}}$  at the NDVI pixel resolution (30 m). Particular interest has the application of this procedure to L5-TM images because of the low contrast shown in the  $LE_d$  results.
- Specific values of soil and canopy emissivities could be assigned to the different land use classes. In this way, emissivity values more representative of the real local vegetation and conditions could be used in the emissivity correction of the radiometric temperature. Also, unique values of  $T_c$  and  $T_s$  have been used for the whole region in the sensible heat fluxes retrieval. An estimation of these values for the different land uses could account for possible differences.

## Conclusions

In this work, a new methodology to estimate actual daily evapotranspiration at a regional scale, assembling remote sensing techniques and ground-measured data, is presented. The traditional relation of Seguin and Itier (1983) is combined with both a balance between the long-wave and the short-wave radiation, to infer the net radiation, and the recently proposed STSEB model, to estimate the sensible heat flux, with the aim of retrieving  $LE_d$  values from single information at a particular day time. The method is applied to the Basilicata region, in the South of Italy. Even though the methodology proposed could be expanded to other satellite sensors, this work is focused on Landsat imagery. Three images acquired in different dates are used in this work, two from Landsat 7-ETM+, and one from Landsat 5-TM. The CORINE Land Cover map and a complete network of agro-meteorological stations provide the set of ground variables and parameters required to apply the methodology. Maps of the different surface fluxes are built up. An analysis of the  $LE_d$  results is made taking the land use classification as a basis, and differences between the different types of vegetation and dates are stated. Overall, the highest  $LE_d$  values correspond to the most vegetated areas. The performance of the method at both local and regional scale is assessed by comparing the results with some ground measurements. An estimation error close to  $1 \text{ mm day}^{-1}$  is finally obtained, in good agreement with other accuracy results shown in the recent literature.

## Acknowledgements

This work was funded by the *Ministerio de Educación y Ciencia* (Project CGL2004-06099-C03-01, co-financed with European Union FEDER funds, *Acciones Complementarias* CGL2005-24207-E/CLI and CGL2006-27067-E/CLI), and the University of Valencia (V Segles Research Grant of Mr.

J.M. Sánchez). The authors express their gratitude to *ALSIA (Agenzia Lucana per lo Sviluppo ed Innovazione in Agricoltura)* for providing field data, to *IMAA (Istituto di Metodologie per l'Analisi Ambientale)* of *CNR (Consiglio Nazionale delle Ricerche)*, and Tito Scalo (PZ) for providing the base elaborations of satellite images, to the *Azienda Agricola Sperimentale Dimostrativa Gaudiano-Lavello(PZ)* and the *Istituto di Scienze delle Produzioni Alimentari of Bari* for providing lysimeters data.

## References

- Anderson, M.C., Norman, J.M., Diak, G.R., Kustas, W.P., Mecikalski, J.R., 1997. A two-source time integrated model for estimating surface fluxes using thermal infrared remote sensing. *Remote Sensing of Environment* 60, 195–216.
- APAT, 2005. The project IMAGE & CORINE Land Cover 2000 in Italy. Final report, April 2005.
- Berk, A., Anderson, G.P., Acharya, P.K., Chetwynd, J.H., Bernstein, L.S., Shettle, E.P., Matthew, M.W., Adler-Golden, S.M., 1999. "MODTRAN 4 user's manual". Air Force Research Laboratory, Space Vehicles Directorate (Hascom AFB, MA: Air Force Materiel Command).
- Chehbouni, A., Nouvellon, Y., Lhomme, J.-P., Watts, C., Boulet, G., Kerr, Y.H., Moran, M.S., Goodrich, D.C., 2001. Estimation of surface sensible heat flux using dual angle observations of radiative surface temperature. *Agricultural and Forest Meteorology* 108, 55–65.
- Choudhury, B.J., Idso, S.B., Reginato, R.J., 1987. Analysis of an empirical model for soil heat flux under a growing wheat crop for estimating evaporation by an infrared-temperature based energy balance equation. *Agricultural and Forest Meteorology* 39, 283–297.
- Cleverly, J., Dahm, C., Thibault, J., Gilroy, D., Coonrod, J., 2002. Seasonal estimates of actual evapotranspiration from Tamarix ramosissima stands using three-dimensional eddy covariance. *Journal of Arid Environments* 52, 181–197.
- Dubayah, R., 1992. Estimating net solar radiation using Landsat Thematic Mapper and digital elevation data. *Water Resource Research* 28, 2469–2484.
- Duguay, C.R., 1992. Estimating surface reflectance and albedo from Landsat-5 thematic Mapper over rugged terrain. *Photogrammetric Engineering & Remote Sensing* 58, 551–558.
- French, A.N., Jacob, F., Anderson, M.C., Kustas, W.P., Timmermans, W., Gieske, A., Su, Z., Su, H., McCabe, M.F., Li, F., Prueger, J., Brunsell, N., 2005. Surface energy fluxes with the Advanced Spaceborne Thermal Emission and Reflection radiometer (ASTER) at the Iowa 2002 SMACEX site (USA). *Remote Sensing of Environment* 99 (1-2), 55–65.
- Gómez, M., Olioso, A., Sobrino, J.A., Jacob, F., 2005. Retrieval of evapotranspiration over the Alpilles/ReSeDA experimental site using airborne POLDER sensor and a thermal camera. *Remote Sensing of Environment* 96, 399–408.
- Humes, K., Ardí, R., Kustas, W.P., Prueger, J., Starks, P., 2002. High Spatial Resolution Mapping of Surface Energy Balance Components with Remotely Sensed Data Thermal Remote Sensing in Land Surface Processes. CRC Press, New York, pp. 110–132.
- Inoue, Y., Moran, M.S., 1997. A simplified method for remote sensing of daily canopy transpiration – a case study with direct measurements of canopy transpiration in soybean canopies. *International Journal of Remote Sensing* 18 (1), 139–152.
- Kustas, W.P., Norman, J.M., Anderson, M., French, A., 2003. Estimating subpixel temperatures and energy fluxes from the vegetation index-radiometric temperature relationship. *Remote Sensing of Environment* 82, 429–440.

- Kustas, W.P., Li, F., Jackson, T.J., Prueger, J.H., MacPherson, J.I., Wolde, M., 2004. Effects of remote sensing pixel resolution on modeled energy flux variability of croplands in Iowa. *Remote Sensing of Environment* 92, 535–547.
- Lagouarde, J.-P., McAneney, K.J., 1992. Daily sensible heat flux estimation from a single measurement of surface temperature and maximum air temperature. *Boundary-Layer Meteorology* 59, 341–362.
- Li, F., Kustas, W.P., Prueger, J.H., Neale, C.M.U., Jackson, T.J., 2005. Utility of Remote Sensing based two-source energy balance model under low and high vegetation cover conditions. *Journal of Hydrometeorology* 6 (6), 878–891.
- McCabe, M.F., Wood, E.F., 2006. Scale influences on the remote estimation of evapotranspiration using multiple satellite sensors. *Remote Sensing of Environment* 105, 271–285.
- Moran, M.S., Clarke, T.R., Inoue, Y., Vidal, A., 1994. Estimating crop water deficit using the relation between surface-air temperature and spectral vegetation index. *Remote Sensing of Environment* 49, 246–263.
- Moran, M.S., Humes, K.S., Pinter, P.J., 1997. The scaling characteristics of remotely sensed variables for sparsely vegetated heterogeneous landscapes. *Journal of Hydrology* 190, 337–362.
- Nagler, P., Cleverly, J., Glenn, E., Lampkin, D., Huete, A., Wan, Z., 2005. Predicting riparian evapotranspiration from MODIS vegetation indices and meteorological data. *Remote Sensing of Environment* 94, 17–30.
- Nagler, P., Jetton, A., Fleming, J., Didan, K., Glenn, E., Erker, J., Morino, K., Milliken, J., Gloss, S., 2007. Evapotranspiration in a cottonwood (*Populus fremontii*) restoration plantation estimated by sap flow and remote sensing methods. *Agricultural and Forest Meteorology* 144, 95–110.
- Ogawa, K., Schmugge, T., Jacob, F., French, A., 2002. Estimation of broadband land surface emissivity from multi-spectral thermal infrared remote sensing. *Agronomie* 22, 695–696.
- Sánchez, J.M., Kustas, W.P., Caselles, V., Anderson, M., 2007a. Modelling surface energy fluxes over maize using radiometric soil and canopy temperature observations. *Remote Sensing of Environment*. doi:10.1016/j.rse.2007.07.018.
- Sánchez, J.M., Caselles, V., Nicolòs, R., Valor, E., Coll, C., Laurila, T., 2007b. Evaluation of the B-method for determining actual evapotranspiration in a boreal forest from MODIS data. *International Journal of Remote Sensing* 28 (5–6), 1231–1250.
- Santanello, J.A., Friedl, M.A., 2003. Diurnal covariation in soil heat flux and net radiation. *Journal of Applied Meteorology* 42, 851–862.
- Scott, R.L., Shuttleworth, W.J., Goodrich, D.C., Maddock III, T., 2000. The water use of two dominant vegetation communities in a semiarid riparian ecosystem. *Agricultural and Forest Meteorology* 105, 241–256.
- Seguin, B., Itier, B., 1983. Using midday surface temperature to estimate daily evaporation from satellite thermal IR data. *International Journal of Remote Sensing* 4 (2), 371–383.
- Sobrino, J.A., Jiménez-Muñoz, J.C., Paolini, L., 2004. Land surface temperature retrieval from LANDSAT TM 5. *Remote Sensing of Environment* 90, 434–440.
- Sobrino, J.A., Gómez, M., Jiménez-Muñoz, J.C., Oliso, A., Chehbouni, G., 2005. A simple algorithm to estimate evapotranspiration from DAIS data: application to the DAISEX campaigns. *Journal of Hydrology* 315, 117–125.
- Su, H., McCabe, M.F., Wood, E.F., Su, Z., Prueger, J.H., 2005. Modelling evapotranspiration during SMACEX02: comparing two approaches for local and regional scale prediction. *Journal of Hydrometeorology* 6 (6), 910–922.
- Valor, E., Caselles, V., 1996. Mapping Land Surface Emissivity from NDVI: application to European, African, and South American areas. *Remote Sensing of Environment* 57, 167–184.
- Valor, E., Caselles, V., 2005. Validation of the vegetation cover method for land surface emissivity estimation. *Recent Research Developments in Thermal Remote Sensing*. Kerala (India), Research Signpost, pp. 1–20.